

Images of Kerr-MOG black holes surrounded by geometrically thick magnetized equilibrium tori

Zelin Zhang^{1*}, Songbai Chen^{1,2†}, Jiliang Jing^{1,2 ‡}

¹*Department of Physics, Institute of Interdisciplinary Studies,
Key Laboratory of Low Dimensional Quantum Structures and Quantum Control of Ministry of Education,
Synergetic Innovation Center for Quantum Effects and Applications,
Hunan Normal University, Changsha, Hunan 410081, People's Republic of China*

²*Center for Gravitation and Cosmology, College of Physical Science and Technology,
Yangzhou University, Yangzhou 225009, People's Republic of China*

Abstract

We adopt general relativistic ray-tracing (GRRT) schemes to study images of Kerr-MOG black holes surrounded by geometrically thick magnetized equilibrium tori, which belong to steady-state solutions of thick accretion disks within the framework of general relativistic magnetohydrodynamics (GRMHD). The black hole possesses an extra dimensionless MOG parameter described its deviation from usual Kerr one. Our results show that the presence of the MOG parameter leads to smaller disks in size, but enhances the total flux density and peak brightness in their images. Combining with observation data of black hole M87* from the Event Horizon Telescope (EHT), we make a constraint on parameters of the Kerr-MOG black hole and find that the presence of the MOG parameter broadens the allowable range of black hole spin.

PACS numbers: 04.70.Dy, 95.30.Sf, 97.60.Lf

* zzl@hunnu.edu.cn

† Corresponding author: csb3752@hunnu.edu.cn

‡ jljing@hunnu.edu.cn

I. INTRODUCTION

General Relativity (GR) has been a fundamental pillar of modern physics, essentially due to its perceived role in black hole physics and cosmology. It provides theoretical explanations for a lot of astronomical phenomena including Mercury's perihelion precession and the dynamics of binary pulsars [1]. With advancements in observational technologies, it is feasible to test GR under extreme conditions. Recent black hole images releasing by the Event Horizon Telescope (EHT) collaborations [2] offer direct evidences of black hole existence in universe, and simultaneously examine validity of GR in strong gravitational fields. However, the current observations cannot completely exclude the possibility of the deviation from GR, which leaves an ample room for other alternative theories of gravity.

The scalar-tensor-vector gravity (STVG) model [3] is a kind of fully covariant modified gravity (MOG) theories. In this MOG theoretical model, there are three gravitational fields: massless tensor graviton, a massless scalar graviton, and a massive vector graviton. It has successfully explained the rotation curves of galaxies [4–6] and the dynamics of galactic clusters [7–9]. The Kerr-like black hole solution in STVG theory is obtained, which owns an extra MOG parameter described the deviation from GR and yielded a variable gravitational constant [10]. Moreover, the MOG parameter describes a new degree of freedom, which influences thermodynamic properties of the black hole [11], dynamical behaviors of particles near the black hole [12–18], and quasinormal modes [19, 20]. It is of interest to study the observational effects of the Kerr-MOG black hole because they could help understand this modified gravity theory. With observations of the S2 star orbiting the supermassive black hole at the Milky Way's center, the MOG parameter α is constrained to $\alpha \lesssim 0.410$ [21]. With the black hole shadows [22–25], the allowed range of the upper limit of the MOG parameter α_{up} is given by $0.350 \lesssim \alpha_{up} \lesssim 0.485$ for the M87* black hole and $0.162 \lesssim \alpha_{up} \lesssim 0.285$ for the SgrA* black hole [26].

Accretion disks are actual and feasible light sources around black holes so the properties of accretion disks have a much greater impact on black hole images. Adopting thin accretion disk model around the Kerr-MOG black hole, it is found that the MOG parameter α influences radiation intensity and the appearance of the black hole images [27, 28]. Moreover, the effects of the MOG parameter α on polarized images arising from a thin accretion disk has been investigated for the rotating black hole [29]. However, above literatures focus only on the thin accretion disk model around MOG black holes. Thus, how thick accretion disk models affect images of the Kerr-MOG black hole is still an open issue. It is well known that studying images of a black hole surrounded by a thick accretion disk must solve general relativistic magnetohydrodynamic

equations of fluids around the black hole. In general, such kind of dynamical equations are very complex so it is very difficult to an analytical solution for them. Thus, the high precise simulation black hole images illuminated by a thick accretion disk must resort numerical GRMHD codes, which expends a significant amount of computing resources. Magnetized equilibrium tori is a kind of simple theoretical models of steady-state geometrically thick accretion disks, which can reveal basic configurations and main features of thick accretion disks through analytical methods. Thus, the magnetized equilibrium tori has applied to simulate millimeter images of Sgr A* [30]. Furthermore, the magnetized equilibrium tori model has also been studied in the spacetimes of deformed compact objects [31], boson stars [32], naked singularities [33], dyonic black holes in quasi-topological electromagnetism [34], and Schwarzschild black holes in swirling universes [35]. In this paper, the main motivation is to study the Kerr-MOG black hole images illuminate by such geometrically thick magnetized equilibrium tori and to probe effects of the MOG parameter on the images.

The paper is organized as follows: In Sec.II, we present an analysis of the magnetized equilibrium tori surrounding a Kerr-MOG black hole. In Sec.III, we simulate images of a Kerr-MOG black hole with magnetized equilibrium tori and to probe effects of the MOG parameter on the images. Finally, we end the paper with a summary.

II. MAGNETIZED EQUILIBRIUM TORI AROUND A KERR-MOG BLACK HOLE

The Kerr-MOG black hole is a stationary axisymmetric solution of field equations within the MOG framework of STVG [10], and its metric form in Boyer-Lindquist coordinates can be expressed as

$$ds^2 = - \left(\frac{\Delta - a^2 \sin^2 \theta}{\Sigma} \right) dt^2 + \frac{\Sigma}{\Delta} dr^2 + \Sigma d\theta^2 - 2 \left(\frac{r^2 + a^2 - \Delta}{\Sigma} \right) a \sin^2 \theta dt d\phi \quad (1)$$

$$+ \left[\frac{(r^2 + a^2)^2 - \Delta a^2 \sin^2 \theta}{\Sigma} \right] \sin^2 \theta d\phi^2, \quad (2)$$

where

$$\Delta = r^2 - 2GMr + a^2 + \alpha GG_N M^2, \quad (3)$$

$$\Sigma = r^2 + a^2 \cos^2 \theta. \quad (4)$$

The parameters a and M represent the black hole's spin and mass, respectively. The MOG parameter α adjusting gravitational constant strength as $G = (1 + \alpha)G_N$, where G_N is Newton-gravitational constant. From now onwards, we adopt $G_N = 1$. The Arnowitt-Deser-Misner (ADM) mass M_α is related to the mass parameter M by $M_\alpha = (1 + \alpha)M$ [14]. With the ADM mass M_α , the outer and inner horizon radii are roots

of the equation

$$\Delta = r^2 - 2M_\alpha r + a^2 + \frac{\alpha}{(1+\alpha)}M_\alpha^2 = 0. \quad (5)$$

and their forms are

$$r_\pm = M_\alpha \pm \sqrt{\frac{M_\alpha^2}{(1+\alpha)} - a^2}. \quad (6)$$

Moreover, the extremal limit for the Kerr-MOG black hole is $M_\alpha^2 = (1+\alpha)a^2$.

To study images of the Kerr-MOG black hole surrounded by geometrically thick magnetized equilibrium tori, we must firstly consider general relativistic magnetohydrodynamics in the curved spacetimes where fluid is dominated by three conservation equations as follows [36],

$$\nabla_\mu T^{\mu\nu} = 0, \quad \nabla_\mu {}^*F^{\mu\nu} = 0, \quad \nabla_\mu \rho u^\mu = 0, \quad (7)$$

where ${}^*F^{\mu\nu}$ is the Faraday tensor and ρ is the rest mass density of fluid. $T^{\mu\nu}$ is the energy-momentum tensor with the form

$$T^{\mu\nu} = (h + b^2)u^\mu u^\nu + (p + \frac{1}{2}b^2)g^{\mu\nu} - b^\mu b^\nu, \quad (8)$$

where h and p correspond to the fluid enthalpy and pressure, respectively. u^μ is the four velocity of fluid and b^μ is the 4-vector form of the magnetic field. For the sake of simplicity, here we assume that the fluid is a barotropic fluid with positive pressure and without self-gravity. Moreover, the fluid is assumed to be axisymmetric and stationary, and the rotation of perfect fluid is restricted to be in the azimuthal direction and the magnetic field in the spacetime is also assumed to be purely azimuthal. With these assumptions, the four velocity of fluid and the four component of the magnetic field can be respectively expressed as

$$u^\mu = (u^t, 0, 0, u^\phi), \quad b^\mu = (b^t, 0, 0, b^\phi). \quad (9)$$

Inserting Eq. (9) into Eqs.(7) and (8), one has [36]

$$\partial_\nu (\ln |u_t|) - \frac{\Omega}{1 - l\Omega} \partial_\nu l + \frac{\partial_\nu p}{h} + \frac{\partial_\nu \tilde{p}_m}{\tilde{h}} = 0, \quad (10)$$

where $\tilde{h} = \mathcal{L}h$ and $\tilde{p}_m = \mathcal{L}p_m$. The factor \mathcal{L} is related to the black hole metric by $\mathcal{L} = g_{t\phi}g_{t\phi} - g_{tt}g_{\phi\phi}$. p_m is the magnetic pressure with the form $p_m = b^2/2$. Here, $\Omega = u^\phi/u^t$ and $l = -u_\phi/u_t$ are respectively the angular velocity and specific angular momentum of the particles in fluid. As in [36], we further assume that the fluid in the magnetized equilibrium tori presents a constant specific angular momentum $l = l_0$ and the corresponding equations of state are

$$p = Kh^\kappa, \quad \tilde{p}_m = K_m \tilde{h}^\eta, \quad (11)$$

where κ and η are two constants. With these assumptions, equation (10) can be integrated as [36]

$$W - W_{in} + \frac{\kappa}{\kappa - 1} \frac{p}{h} + \frac{\eta}{\eta - 1} \frac{p_m}{h} = 0. \quad (12)$$

Here W is the potential with the form

$$W(r, \theta) = \frac{1}{2} \ln \left| \frac{\mathcal{L}}{\mathcal{A}} \right|. \quad (13)$$

where $\mathcal{A} = g_{\phi\phi} + 2l_0 g_{t\phi} + l_0^2 g_{tt}$. The quantity W_{in} denotes the value of the potential at the inner edge of the disk. With these equations, we can analyze the structures and properties of geometrically thick magnetized equilibrium tori around the Kerr-MOG black hole.

The value of l_0 plays a pivotal role in the potential W which determines the topology and structures of the equilibrium tori. Here we set the constant specific angular momentum $l_{ms} < l_0 < l_{mb}$, where l_{ms} and l_{mb} are respectively the specific angular momentum of the fluid particles moving along the marginally stable circular orbit r_{ms} and the marginally bound orbit r_{mb} . The main reason is that the existence of magnetized equilibrium tori around black holes requires that the value of l_0 in the fluid must satisfy $l_0 > l_{ms}$ [36]. Meanwhile, the condition $l_0 < l_{mb}$ ensures that the equilibrium tori have a cusp and a center, which could bring richer features for black hole images. Therefore, the potential $W(r, \theta)$ inside the disk usual satisfies $W_c < W(r, \theta) < W_{cusp}$, where W_c and W_{cusp} respectively correspond to the potential at the disk's center and at the cusp. For the convenience, one can introduce the dimensionless specific angular momentum

$$\lambda \equiv \frac{l_0 - l_{ms}}{l_{mb} - l_{ms}}, \quad (14)$$

and the dimensionless potential

$$w(r, \theta) = \frac{W(r, \theta) - W_{cusp}}{W_c - W_{cusp}}. \quad (15)$$

It is obvious that these two dimensionless parameters satisfy $0 < \lambda < 1$ and $0 \leq w(r, \theta) \leq 1$, respectively. Similarly, we recast W_{in} in terms of the dimensionless parameter as $w_{in} = (W_{in} - W_c)/(W_{cusp} - W_c)$. In order to obtain the distribution of enthalpy h and pressure p in the magnetized equilibrium tori for fixed κ and η , we must firstly get the gas pressure and the magnetic pressure at the disk's center $r = r_c$, i.e., [36]

$$p_c = h_c w_{in} (W_{cusp} - W_c) \left(\frac{\kappa}{\kappa - 1} + \frac{\eta}{\eta - 1} \frac{1}{\beta_c} \right)^{-1}, \quad p_{m_c} = p_c / \beta_c, \quad (16)$$

where h_c and $\beta_c = (p/p_m)_c$ denote the enthalpy and the plasma magnetization parameter at the disk's center, respectively. With Eqs.(16), the constants K and K_m in equation (11) can be given. Solving Eq.(12), we can

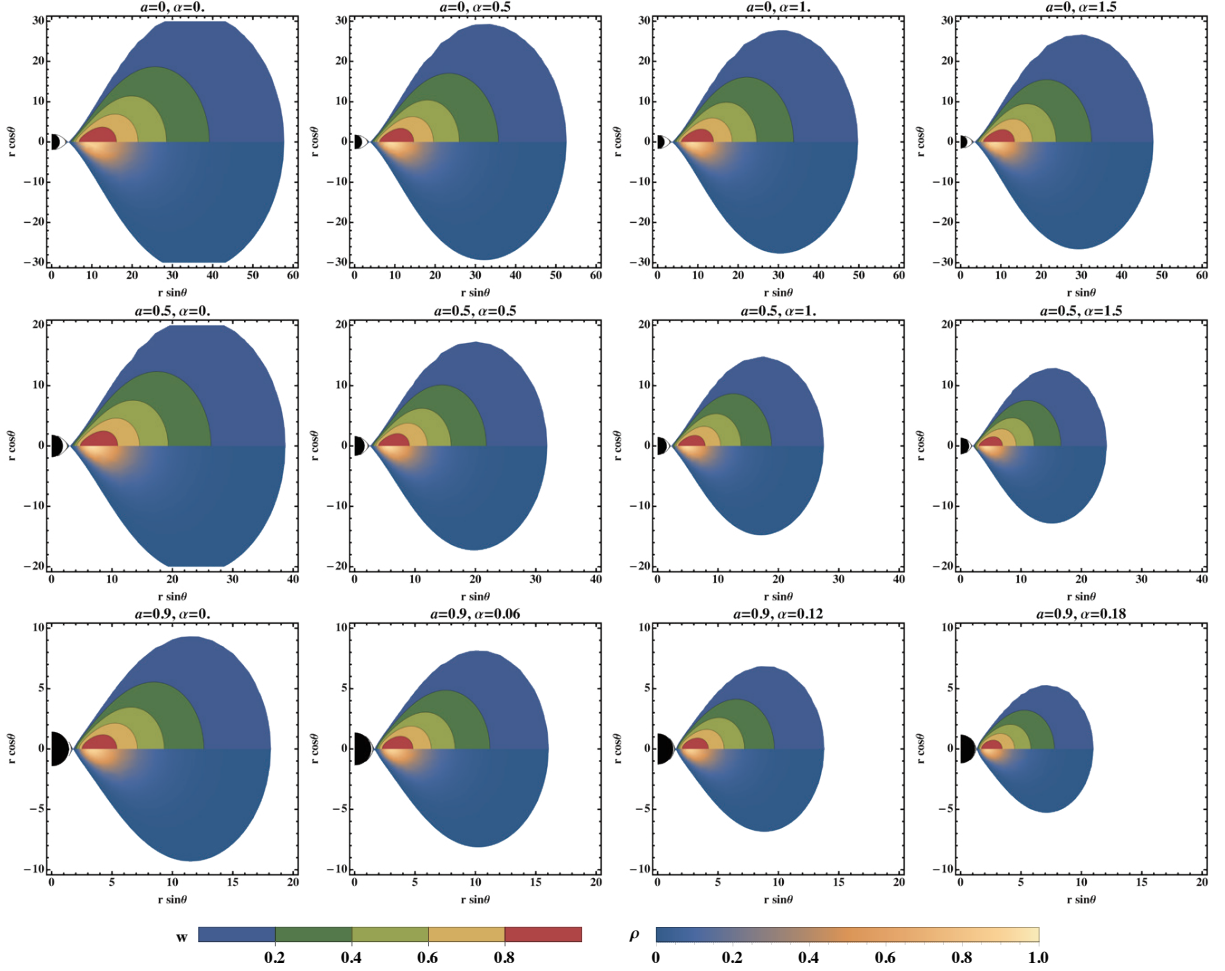


FIG. 1: Dimensionless potential and density distribution in the geometrically thick magnetized equilibrium tori around Kerr-MOG black holes with different spin and MOG parameters. In each panel, the upper half and the lower one depict the dimensionless potential and the rest mass density distribution, respectively.

get the distribution of enthalpy h and pressure p in the magnetized equilibrium tori. The rest mass density in the tori can be further given by

$$\rho = h - \frac{\kappa p}{\kappa - 1}. \quad (17)$$

In general, the regions in accretion disk around black holes is weakly magnetized accretion disks with high β , where $\beta \equiv p/p_m$ is the plasma magnetization parameter [37, 38]. Fig. 1 presents the geometrically thick magnetized equilibrium tori around the Kerr-MOG black hole, where we set $\beta_c = 10$, $h_c = 1$, $w_{in} = 1$, $\lambda = 0.8$ and $\kappa = \eta = 4/3$. One can find that the dimensionless potential w reaches its maximums at the tori centers and drop to zero at its outermost surface. The rest mass density distribution is similar to that of the potential w , but the rest mass density ρ own more rapidly rate of decay with the distance from the center. Moreover, both the black hole spin a and the MOG parameter α lead to the sharp decrease in the size of equilibrium

tori. However, the shape of equilibrium tori is not susceptible to these two parameters.

III. SIMULATED IMAGES OF MAGNETIZED EQUILIBRIUM TORI

To simulate images of geometrically thick magnetized equilibrium tori around the Kerr-MOG black hole, here we assume that the equilibrium tori are low-density and high-temperature, where the plasma is collisionless and the electron temperature T_e is lower than the ion temperature T_i as in [39]. The electron temperature directly affects synchrotron radiation emission in the tori. Following the model in [38], the electron temperature T_e is assumed as

$$T_e = \frac{2m_p u}{3k_B \rho(2 + R)}, \quad (18)$$

which depends on the plasma density ρ , the internal energy density u , the magnetization parameter β and the proton mass m_p . Here k_B is Boltzmann's constant and $R \equiv T_i/T_e$ is the proton-to-electron temperature ratio with a form

$$R = R_{high} \frac{\beta^2}{1 + \beta^2} + \frac{1}{1 + \beta^2}, \quad (19)$$

which means that the ratio R can be adjusted by the parameter R_{high} and the plasma magnetization parameter β in the tori. The internal energy density u can be obtained by the pressure p using the relation $u = p/(\kappa - 1)$. As in [38], for matching simulation images with actual observed images, one can introduce a scaling factor \mathcal{M} , which can adjust physical properties in magnetized equilibrium tori including the rest mass density, the magnetic field strength and the internal energy density, and further impacts the flux density in the simulated images.

To numerically simulate the radiative transfer within the magnetized equilibrium tori around black holes, we utilize the **ARCMANCER** library [40], where the emission, absorption, and Faraday mixing coefficients of radiation in the magnetized plasma are calculated by employing the **symphony** code [41–43]. Here, we focus only on the case where electrons are in thermal distributions and the corresponding radiative flux is produced only by thermal synchrotron emission. In this work, we set $R_{high} = 10$ to model the electron temperature and adopt the M87* black hole as a target with black hole mass $6.5 \times 10^9 M_\odot$ and the observer's distance $r_0 = 16.8 \text{ kpc}$ to simulate black hole images at the observation frequency 230GHz [2, 44]. Fig.2 presents the simulated images of the Kerr-MOG black hole for fixed spin parameter $a = 0.5$ with different MOG parameter α and observed inclination angle θ . The images show that there are closely-packed bright thin rings together with a crescent-shaped bright zone. The crescent-shaped bright zone corresponds to the primary image of the

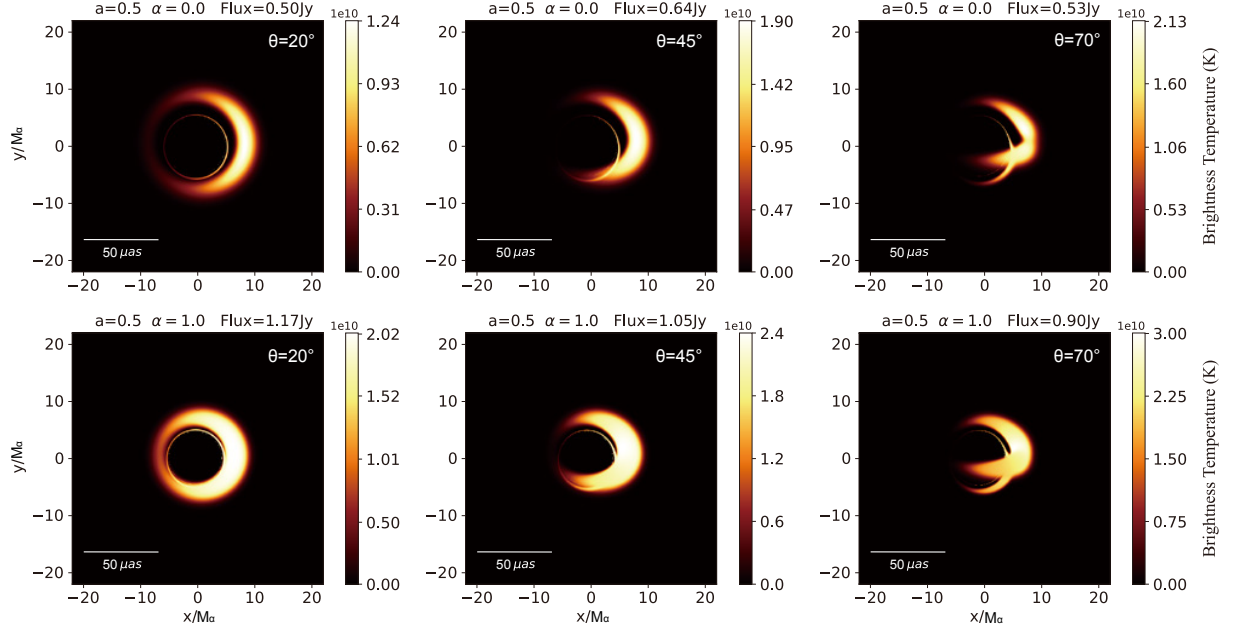


FIG. 2: Simulated images of geometrically thick magnetized equilibrium tori around Kerr-MOG black hole for fixed spin parameter $a = 0.5$ with different MOG parameter α and observed inclination angle θ . The images are presented in units of brightness temperature $T_b = S\lambda^2/(2k_B\Omega)$, where S denotes the flux density, λ is the observing wavelength and Ω the solid angle subtended by the resolution element.

magnetized equilibrium tori. The bright thin rings denote higher-order images of tori arising from light rays crossing the tori multiple times before reaching observation. From Fig.2, for different observer's inclination angle, we find that with the increasing of the MOG parameter α , both the brightness temperatures and the radiative flux increase, but the size of the images decreases. The latter can be explained by a fact that the size of the magnetized equilibrium tori decreases with the parameter α . Moreover, we also find that the width of the crescent-shaped bright zone increases with α . In order to compare with the observed image of the black hole M87*, in Fig. 3, we presents simulated images of geometrically thick magnetized equilibrium tori around a Kerr-MOG black hole with an observation inclination angle $\theta = 17^\circ$ and a position angle (PA) of 288° [45, 46]. In this special case with observation inclination angle $\theta = 17^\circ$, we find that the changes of equilibrium tori images with the MOG parameter are similar to those shown in Fig. 2. However, we also find that in the cases with non-zero α , the image's size decays more rapidly with the spin parameter a .

In Fig.4, we also presents blurred images of geometrically thick magnetized equilibrium tori around a Kerr-MOG black hole for the images in Fig.3 through convolving with a $20\mu as$ FWHM Gaussian beam, which is convenient to compare with the current EHT observational images for the black hole M87* due to its limited resolution [2, 38, 44]. As illustrated in Fig.4, the thin bright ring in the image disappears due to the blurring process, and the crescent-shaped bright zone becomes more broaden, which yields that features of the blurred

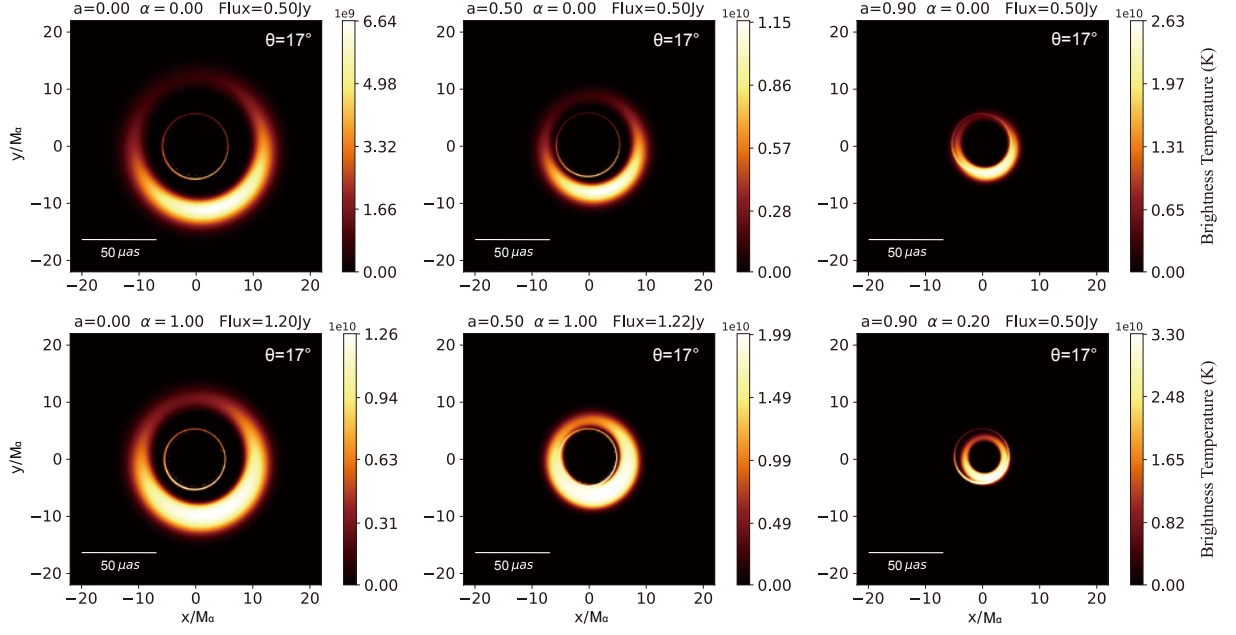


FIG. 3: Simulated images of geometrically thick magnetized equilibrium tori around a Kerr-MOG black hole with different MOG parameter α and spin parameter a . The observed inclination is set to $\theta = 17^\circ$ and the position angle (PA) is 288° .

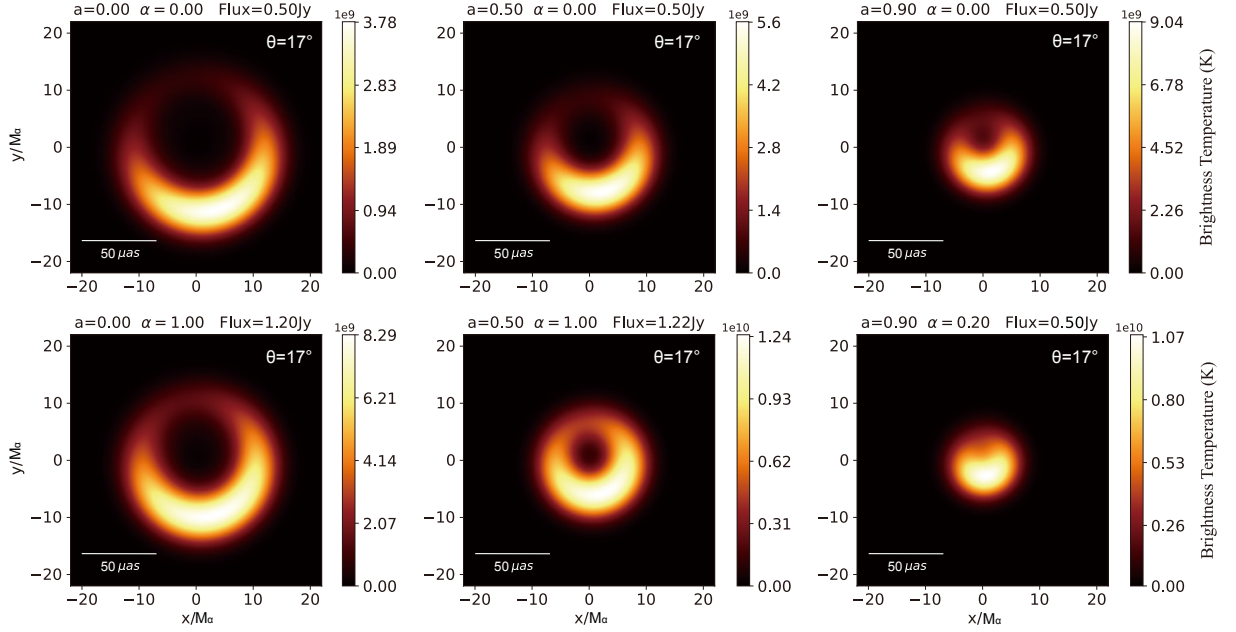


FIG. 4: Blurred images of geometrically thick magnetized equilibrium tori around a Kerr-MOG black hole for the images in Fig.3 through convolving with a $20\mu\text{as}$ FWHM Gaussian beam.

images are highly consistent with those of observed black hole images [2, 44]. The size of the bright rings is evidently influenced by the black hole spin a and the MOG parameter α , which implies that images of Kerr-MOG black hole can be compatible with the observed image of the black hole M87* by tuning these two parameters. However, we find that images of Kerr-MOG black hole are highly overlapping for certain

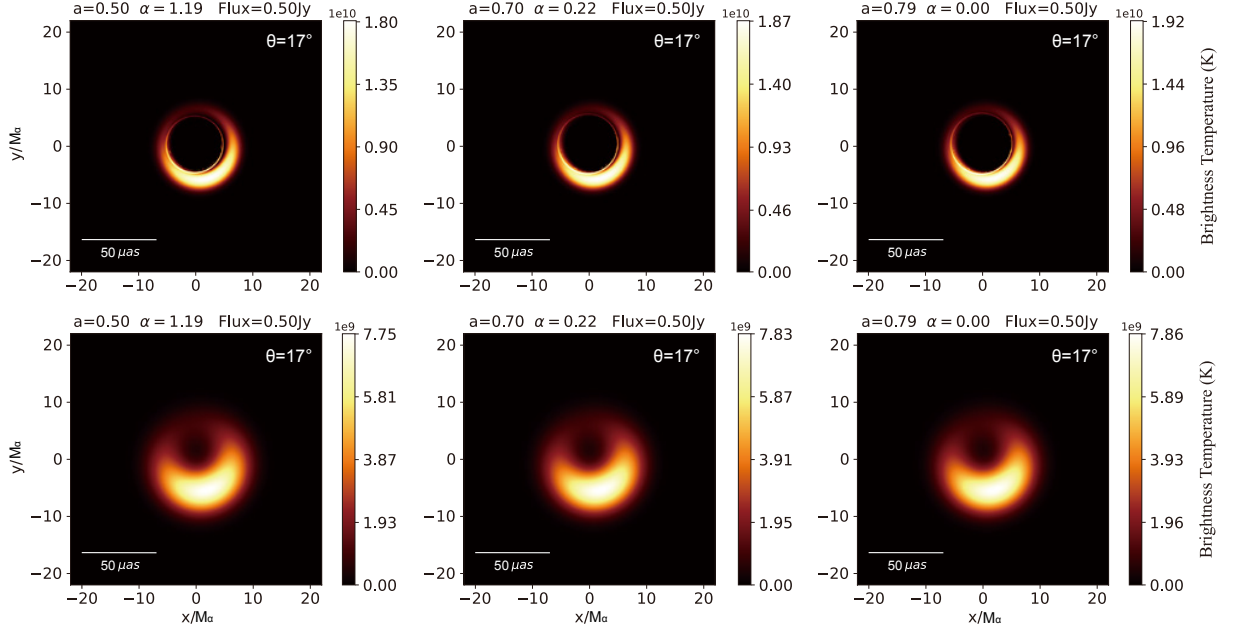


FIG. 5: Highly overlapping of Kerr-MOG black hole images for three distinct parameter sets of a and α . Here the diameters of the bright rings are set $d = 43.3\mu\text{as}$.

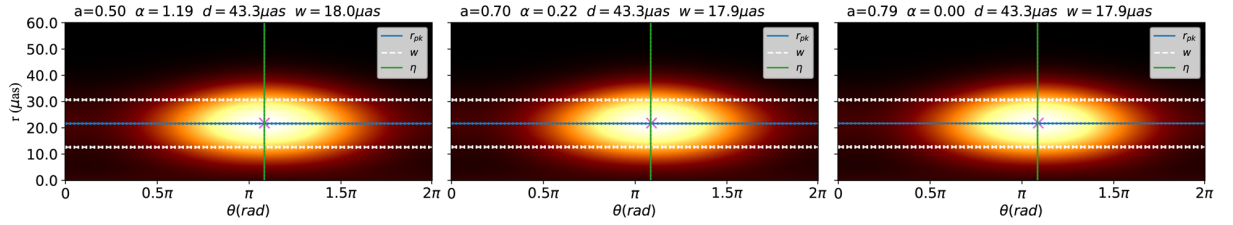


FIG. 6: Unwrapped ring profiles of the simulated images in Fig.5. The estimated radius $d/2$ is shown with a horizontal line, with dotted lines denoting the associated uncertainty. Horizontal dashed lines at $(d \pm w)/2$ show the measured ring width. Vertical green lines give the orientation angle η and its uncertainty. The purple cross marks the peak brightness in each panels.

parameter sets of a and α , so that the simulated images are practically indistinguishable from each other, which is shown in Fig.5. Moreover, for these highly overlapping Kerr-MOG black hole images for three different parameter sets, the corresponding equilibrium tori share the identical electron density $n_e \sim 2 \times 10^6 \text{ cm}^{-3}$, electron temperatures $T_e \sim 3 \times 10^{10} \text{ K}$, and magnetic field strengths $B \sim 11 \text{ G}$. Moreover, our results also show that the Kerr black hole images can overlap with those of Kerr-MOG black holes with the lower spin parameter a due to the presence of the MOG parameter α . These overlapping images lead to a challenge for us to identify black hole parameters by using of black hole images. Following the methodology in [47], in Fig.6, we present the unwrapped ring profiles of the simulated images, which clearly show that Kerr-MOG black hole images for three different parameter sets selected in Fig.5 have the same diameters of the bright rings $d = 43.3 \mu\text{as}$ as observed in the black hole M87* images [44]. As in ref [2, 47], the ring widths in the

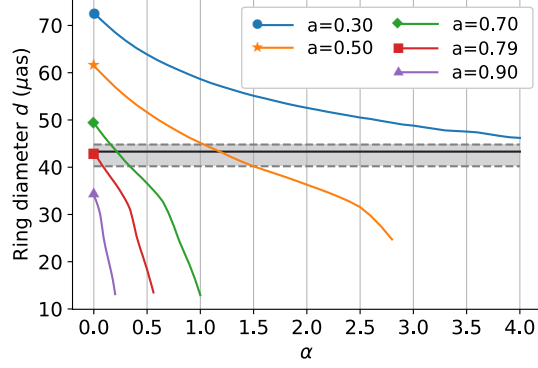


FIG. 7: Ring diameters varies with the α parameter for different spin parameters $a = 0.3, 0.5, 0.7, 0.79$ and 0.9 . The observed $43.3\mu\text{as}$ diameter in M87* [44] is denoted by a central black line and the gray region corresponds to the 1-sigma uncertainty range.

simulated images are approximately $w \sim 18 \mu\text{as}$, which falls within the observational constraint $w < 20 \mu\text{as}$.

Fig.7 presents the allowed range of the MOG parameter α and spin parameter a for the Kerr-MOG black hole in term of the bright ring diameter of the M87* images. Here, the central black line represents the M87* observed ring diameter as $43.3 \mu\text{as}$ and the gray region denotes the 1-sigma uncertainty range [44]. Fig.7 shows that the presence of the MOG parameter α broadens the allowed range of the spin parameter a .

IV. SUMMARY

We have firstly studied geometrically thick magnetized equilibrium tori around a Kerr-MOG black hole with an extra MOG parameter α . We find that both the black hole spin a and the MOG parameter α lead to the sharp decrease in the size of equilibrium tori, but the shape of equilibrium tori is not susceptible to these two parameters. Moreover, the rest mass density distribution is similar to that of the potential w , but the rest mass density ρ own more rapidly rate of decay with the distance from the center. Then, we simulated the images of Kerr-MOG black holes surrounded by the geometrically thick magnetized equilibrium tori. The images show that there are closely-packed bright thin rings together with a crescent-shaped bright zone. With the increasing of the MOG parameter α , both the brightness temperatures and the radiative flux increase, but the size of the images decreases. Moreover, we also find that the width of the crescent-shaped bright zone increases with α . Due to the presence of the MOG parameter α , the image's size decays more rapidly with the spin parameter a . Especially, we find that images of Kerr-MOG black hole can be highly overlapping for certain parameter sets of a and α , which lead to a challenge for us to identify black hole parameters by using of black hole images. Finally, we presents the allowed range of the MOG parameter α and spin parameter a

for the Kerr-MOG black hole in term of the bright ring diameter of the M87* images, which shows that the presence of the MOG parameter α broadens the allowed range of the spin parameter a . These results could help us to deeply understand black hole images and the Kerr-MOG black hole in the scalar-tensor-vector gravity theory.

V. ACKNOWLEDGMENTS

This work was supported by the National Natural Science Foundation of China under Grant No.12275078, 11875026, 12035005, 2020YFC2201400, and the innovative research group of Hunan Province under Grant No. 2024JJ1006.

-
- [1] C. M. Will, *Living Reviews in Relativity* **17**, 4 (2014), 1403.7377.
 - [2] Event Horizon Telescope Collaboration, K. Akiyama, A. Alberdi, W. Alef, K. Asada, R. Azulay, A.-K. Baczko, D. Ball, M. Baloković, J. Barrett, et al., *ApJ* **875**, L1 (2019), 1906.11238.
 - [3] J. W. Moffat, *J. Cosmology Astropart. Phys.* **2006**, 004 (2006), gr-qc/0506021.
 - [4] J. W. Moffat and S. Rahvar, *MNRAS* **436**, 1439 (2013), 1306.6383.
 - [5] Z. Davari and S. Rahvar, *MNRAS* **496**, 3502 (2020), 2006.06032.
 - [6] J. W. Moffat and V. T. Toth, *MNRAS* **527**, 2687 (2024), 2308.09838.
 - [7] J. W. Moffat and V. T. Toth, *MNRAS* **397**, 1885 (2009), 0805.4774.
 - [8] J. W. Moffat and S. Rahvar, *MNRAS* **441**, 3724 (2014), 1309.5077.
 - [9] N. S. Israel and J. W. Moffat, *arXiv e-prints arXiv:1606.09128* (2016), 1606.09128.
 - [10] J. W. Moffat, *European Physical Journal C* **75**, 175 (2015), 1412.5424.
 - [11] J. R. Mureika, J. W. Moffat, and M. Faizal, *Physics Letters B* **757**, 528 (2016), 1504.08226.
 - [12] M. Sharif and M. Shahzadi, *European Physical Journal C* **77**, 363 (2017), 1705.03058.
 - [13] H.-C. Lee and Y.-J. Han, *European Physical Journal C* **77**, 655 (2017), 1704.02740.
 - [14] P. Sheoran, A. Herrera-Aguilar, and U. Nucamendi, *Phys. Rev. D* **97**, 124049 (2018), 1712.03344.
 - [15] K. Haydarov, J. Rayimbaev, A. Abdujabbarov, S. Palvanov, and D. Begmatova, *European Physical Journal C* **80**, 399 (2020), 2004.14868.
 - [16] J. Rayimbaev, P. Tadjimuratov, A. Abdujabbarov, B. Ahmedov, and M. Khudoyberdieva, *Galaxies* **9**, 75 (2021), 2010.12863.
 - [17] S. Murodov, J. Rayimbaev, B. Ahmedov, and A. Hakimov, *Symmetry* **15**, 2084 (2023), 2310.08046.
 - [18] S. Ullah Khan, J. Rayimbaev, Z.-M. Chen, and Z. Stuchlík, *arXiv e-prints arXiv:2311.16936* (2023), 2311.16936.
 - [19] L. Manfredi, J. Mureika, and J. Moffat, *Physics Letters B* **779**, 492 (2018), 1711.03199.
 - [20] W. Liu, X. Fang, J. Jing, and J. Wang, *J. Cosmology Astropart. Phys.* **2023**, 057 (2023), 2306.03599.
 - [21] R. Della Monica, I. de Martino, and M. de Laurentis, *Universe* **8**, 137 (2022), 2206.12699.
 - [22] J. W. Moffat, *European Physical Journal C* **75**, 130 (2015), 1502.01677.
 - [23] H.-M. Wang, Y.-M. Xu, and S.-W. Wei, *J. Cosmology Astropart. Phys.* **2019**, 046 (2019), 1810.12767.
 - [24] J. W. Moffat and V. T. Toth, *Phys. Rev. D* **101**, 024014 (2020), 1904.04142.
 - [25] S. Hu, C. Deng, D. Li, X. Wu, and E. Liang, *European Physical Journal C* **82**, 885 (2022).
 - [26] X.-M. Kuang, Z.-Y. Tang, B. Wang, and A. Wang, *Phys. Rev. D* **106**, 064012 (2022), 2206.05878.
 - [27] D. Pérez, F. G. L. Armengol, and G. E. Romero, *Phys. Rev. D* **95**, 104047 (2017), 1705.02713.
 - [28] S. Hu, C. Deng, S. Guo, X. Wu, and E. Liang, *European Physical Journal C* **83**, 264 (2023).
 - [29] X. Qin, S. Chen, Z. Zhang, and J. Jing, *ApJ* **938**, 2 (2022), 2207.12034.
 - [30] F. H. Vincent, W. Yan, O. Straub, A. A. Zdziarski, and M. A. Abramowicz, *A&A* **574**, A48 (2015), 1406.0353.
 - [31] S. Faraji and A. Trova, *A&A* **654**, A100 (2021), 2011.05945.
 - [32] K. Gjorgjeski, J. Kunz, M. C. Teodoro, L. G. Collodel, and P. Nedkova, *Phys. Rev. D* **107**, 103043 (2023), 2301.00449.
 - [33] G. D. Prada-Méndez, F. D. Lora-Clavijo, and J. M. Velásquez-Cadavid, *Classical and Quantum Gravity* **40**, 195011 (2023), 2308.09174.
 - [34] X. Zhou, S. Chen, and J. Jing, *European Physical Journal C* **84**, 130 (2024), 2307.01996.
 - [35] C. Chen, Q. Pan, and J. Jing, *arXiv e-prints arXiv:2402.02789* (2024), 2402.02789.
 - [36] S. S. Komissarov, *MNRAS* **368**, 993 (2006), astro-ph/0601678.
 - [37] M. Mościbrodzka, H. Falcke, and H. Shiokawa, *A&A* **586**, A38 (2016), 1510.07243.

- [38] Event Horizon Telescope Collaboration, K. Akiyama, A. Alberdi, W. Alef, K. Asada, R. Azulay, A.-K. Bacsko, D. Ball, M. Baloković, J. Barrett, et al., *ApJ* **875**, L5 (2019), 1906.11242.
- [39] F. Yuan and R. Narayan, *ARA&A* **52**, 529 (2014), 1401.0586.
- [40] P. Pihajoki, M. Mannerkoski, J. Nättilä, and P. H. Johansson, *ApJ* **863**, 8 (2018), 1804.04670.
- [41] A. Pandya, Z. Zhang, M. Chandra, and C. F. Gammie, *ApJ* **822**, 34 (2016), 1602.08749.
- [42] A. Pandya, M. Chandra, A. Joshi, and C. F. Gammie, *ApJ* **868**, 13 (2018), 1810.05530.
- [43] A. Marszewski, B. S. Prather, A. V. Joshi, A. Pandya, and C. F. Gammie, *ApJ* **921**, 17 (2021), 2108.10359.
- [44] Event Horizon Telescope Collaboration, K. Akiyama, A. Alberdi, W. Alef, J. C. Algaba, R. Anantua, K. Asada, R. Azulay, U. Bach, A.-K. Bacsko, et al., *A&A* **681**, A79 (2024).
- [45] R. C. Walker, P. E. Hardee, F. B. Davies, C. Ly, and W. Junor, *ApJ* **855**, 128 (2018), 1802.06166.
- [46] Y. Cui, K. Hada, T. Kawashima, M. Kino, W. Lin, Y. Mizuno, H. Ro, M. Honma, K. Yi, J. Yu, et al., *Nature* **621**, 711 (2023), 2310.09015.
- [47] Event Horizon Telescope Collaboration, K. Akiyama, A. Alberdi, W. Alef, K. Asada, R. Azulay, A.-K. Bacsko, D. Ball, M. Baloković, J. Barrett, et al., *ApJ* **875**, L4 (2019), 1906.11241.